Feasibility of Monochromatic X-ray Imaging of the Near-Field Region of an Airblast Atomizer

T. B. Morgan[1*], J. K. Bothell[1], D. Li[1], T. J. Heindel[1],
A. Aliseda[2], N. Machicoane[2], A. L. Kastengren[3]
[1]Department of Mechanical Engineering, Iowa State University, USA
[2]Department of Mechanical Engineering, University of Washington, USA
[3]X-ray Science Division, Argonne National Laboratory, USA

Abstract

The characterization of the atomization process in a spray is critical to improving the efficiency and effectiveness of sprays across a wide variety of industries. The near-field region of the spray is particularly important in this characterization as it provides insight into the mechanisms that drive droplet formation. Unfortunately, this region is also difficult to image due to its inaccessibility to optical techniques and the high speed of the events of interest. X-ray measurement techniques, such as white beam and focused beam radiography measurements, have been used to penetrate this dense liquid region and provide useful information.

This paper presents a modification of the white beam measurement technique and investigates the feasibility of completing monochromatic X-ray radiography using the 7-BM beamline at the Advanced Photon Source at Argonne National Laboratory. Monochromatic X-ray radiography allows for the direct calculation of the effective path length at any location in the imaging area, but typically has a very low intensity, which has traditionally limited its use to point measurements (e.g., focused beam measurements). In order to demonstrate the potential and challenges of monochromatic beam radiography, time-resolved monochromatic X-ray images of a simple liquid stream and a low velocity spray from an airblast atomizer were acquired. Using these representative test data, it is shown that the monochromator used to generate the monochromatic beam introduced a non-uniform, time-varying, systematic imaging error. This error and its effect on the measurements will be demonstrated and discussed.

Keywords: Airblast Atomizer, Effective Path Length, Synchrotron Radiation, X-ray Imaging

Introduction

In order to improve the efficiency and effectiveness of sprays, it is important to understand the dynamics in the near-field region of the spray, as the phenomena that drive droplet formation occur in this region. Unfortunately, this region of the spray is also difficult to characterize experimentally as the high liquid concentration makes the region optically dense, and the high speeds involved in droplet formation events necessitate high frequency measurement. One method that has been successful in experimentally characterizing this region is X-ray measurement techniques, such as white beam and focused beam radiography, which are capable of penetrating through the dense liquid in the region [1,2]. Synchrotron X-ray sources, in particular, have the advantage of having high flux, photon energy tunability, and a highly collimated beam [2].

Previous studies using synchrotron X-ray sources to study sprays have used multiple techniques to investigate the flow characteristics including phase contrast imaging, X-ray fluorescence, and radiography [2]. The studies using radiography have generally used two different approaches [3–5]. One approach (referred to here as white beam radiography) is to use the polychromatic white beam produced by the synchrotron source, coupled with an imaging X-ray detector to produce a sequence of still frames of the flow. This method provides information about numerous spatial positions during an individual time period, but the use of a polychromatic beam makes the calculation of the effective X-ray path length challenging [5]. The second commonly used method (referred to here as focused beam radiography) uses a monochromator and focusing mirrors to produce an extremely small, but intense, X-ray beam that can be used to measure the spray at an extremely high speed, but only at a single spatial point. Thus, the beam must be raster scanned through the flow field to provide spatial information, as well as phase-locked to capture any periodic events [3].

A middle ground between white beam radiography and focused beam radiography is monochromatic beam radiography (or mono beam radiography). In mono beam radiography, a monochromator is inserted into the white beam to produce a monochromatic X-ray beam (like focused beam radiography); however, no focusing mirrors are

* Corresponding author, tbmorgan@iastate.edu

used (like white beam radiography), resulting in a larger X-ray beam that can be used with an imaging X-ray detector. Hence, knowing the wavelength of the monochromatic beam, the effective path length (EPL) through the spray can be determined precisely in the entire imaging region. The drawback of this system is that the monochromatic beam has a very low intensity compared to the raw white beam from the synchrotron source. Additionally, unlike focused beam radiography, mono beam radiography is subject to the same phase-contrast effects that occur in white beam imaging, which can reduce the accuracy of EPL calculations near phase boundaries. Finally, as described below, vibrations occur in the monochromator during use, which introduces a time and position dependent variation in the X-ray beam intensity. This paper examines the practical effects of these variations on the usefulness of mono beam radiography for spray characterization.

Experimental Methods

The experiments in this study were conducted at the 7-BM beamline of the Advanced Photon Source (APS) at Argonne National Laboratory. The 7-BM beamline produces a polychromatic X-ray beam by bending the path of high energy (7 GeV) electrons in the storage ring of the synchrotron using a bending magnet. This beam is filtered to a narrow range of energies (8 keV mean energy, 4% ΔE/E, for this study) using a monochromator. This monochromatic X-ray beam is then passed through the spray of interest and onto a 500 µm thick cerium-doped yttrium aluminum garnet (YAG:Ce) scintillator. The scintillator converts the X-ray light into visible light which is then imaged with a Photron FASTCAM Mini AX50 high speed camera via a mirror and lens (a 105 mm lens and a 50 mm lens connected front to front with a macro coupler). This process is illustrated in the schematic in Figure 1.

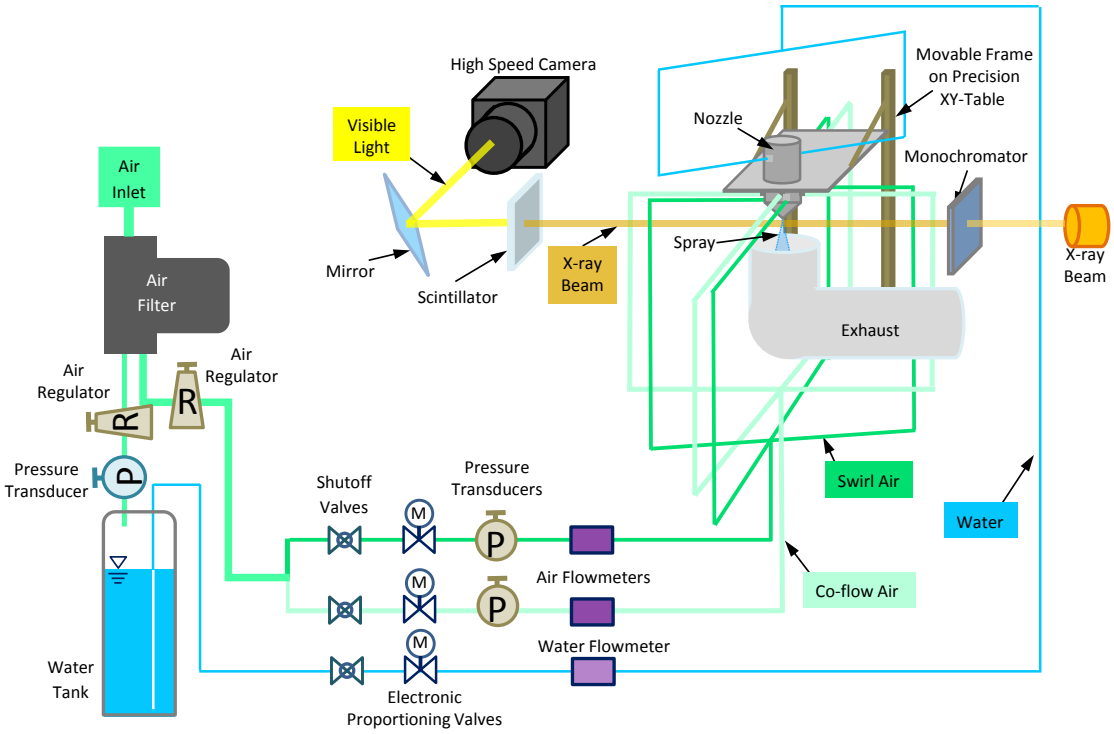

Figure 1 Schematic of the airblast atomizer setup for monochromatic beam imaging at the 7-BM beamline at the Advanced Photon Source.

In this study, a canonical coaxial flow airblast atomizer was used. It consists of an inner liquid nozzle (inner diameter 2.1 mm, outer diameter 2.7 mm), surrounded by a coaxial air nozzle (outer diameter of 10 mm), and is identical to the airblast atomizer used by [6–8]. The liquid flow rate (Q_l) and the straight coaxial gas flow rate of the nozzle (Q_g) are each measured with an electronic flow meter which in turn drives an electronically controlled proportional valve using a proportional-integral-derivative (PID) controller. A PID controlled swirl gas flow is also available; however, it was not used in this study. The liquid used in this study was distilled water, and the gas used was air. This atomizer is described in more detail in [6].

The liquid Reynolds number for the airblast atomizer is defined as:

$$Re_l = \frac{U_l D_i}{\nu_l} \tag{1}$$

where U_l is the mean liquid velocity, D_i is the inner diameter of the liquid nozzle (2.1 mm), and ν_l is the kinematic viscosity of the liquid. Similarly, the gas Reynolds number for the atomizer is defined as:

$$Re_g = \frac{U_g D_h}{\nu_g} \tag{2}$$

where U_g is the mean gas velocity, ν_g is the kinematic viscosity of the gas, and D_h is the hydraulic diameter of the gas nozzle, which is defined as:

$$D_h = D_{g,o} - D_{g,i} \tag{3}$$

where $D_{g,o}$ is the outer diameter of the gas nozzle (10 mm) and $D_{g,i}$ is the inner diameter of the gas nozzle (which is the same as the outer diameter of the liquid nozzle, 2.7 mm).

For the test conditions in this study, the high speed camera acquired images at a pixel resolution of 736 × 256 and a frame rate of 3600 Hz or 7200 Hz, depending on the flow of interest. These frames cover a spatial area of 7.010 mm horizontally and 2.438 mm vertically; however, only 2.124 mm of height is usable due to the size of the X-ray beam. Because the X-ray beam is monochromatic, the Beer-Lambert law for the X-ray attenuation simplifies to:

$$I = I_0 e^{-\left(\frac{\mu}{\rho}\right)\rho l} \tag{4}$$

where I_0 is the initial X-ray intensity, $\left(\frac{\mu}{\rho}\right)$ is the mass attenuation coefficient of the material, ρ is the density of the material, and l is the EPL through the spray. The mass attenuation coefficient (at the specific energy level of the monochromatic beam, 8 keV) and the density of the liquid are readily available quantities and the initial X-ray intensity can be obtained by imaging the X-ray beam with no spray in the imaging region [9]. Thus, the EPL of liquid through which the X-ray traveled, assuming the X-ray attenuation of the gas is negligible, can be calculated by:

$$l = \frac{\ln \frac{I}{I_0}}{-\left(\frac{\mu}{\rho}\right)\rho} \tag{5}$$

Results and Discussion

One of the key assumptions in Equation (5) is that the initial X-ray beam intensity (I_0) does not change between when the reference images are acquired and when the data images are acquired. Unfortunately, in mono beam radiography, this assumption is violated. A combination of the motions of the X-ray source and the vibration of the monochromator optics introduces a time dependent spatial variation in the beam intensity [10]. Specifically, the background of the image moves vertically a small amount. This spatial variation is shown without an overlaying spray in Figure 2, and the approximate vertical displacement from the first frame in the sequence is shown in Figure 3. The vertical displacement was approximated using a cross-correlation between the first frame and the nth frame in the sequence. The variation has two important properties that make it particularly difficult to

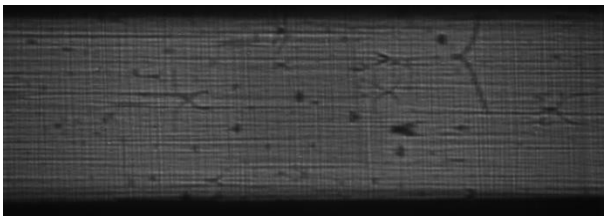

Figure 2 A single frame of the spatial variation in the initial X-ray intensity caused primarily by the monochromator. This frame covers a physical area of 7.0 mm wide by 2.4 mm high.

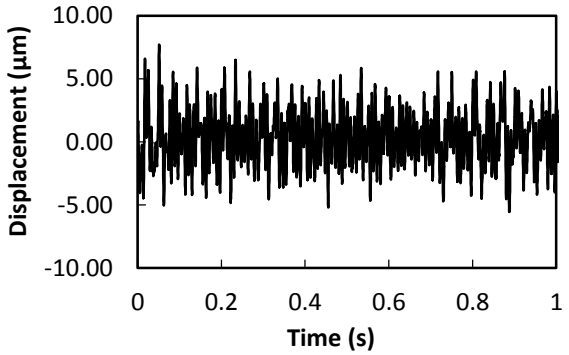

Figure 3 The approximate vertical displacement of the background intensity due to vibrations in the monochromator.

remove from the data using traditional image processing techniques. First, the motion of the background is not periodic (the power spectrum of the motion is roughly pink noise); therefore, the position of the background cannot be predicted. Second, the amplitude of the deviation is consistently less than one pixel (9.52 μm). Because of this low amplitude, any attempt to measure and correct for the moving background is subject to significant interpolation effects. The result of this uncorrected variation is a systematic error in the resulting EPL due to the inability to fully represent the initial X-ray intensity. However, in spite of this error, mono beam radiography is still capable of making useful measurements, and will improve as better correction methods are developed.

To demonstrate the advantages and limitations of mono beam radiography, two example flow conditions were tested. The first flow condition was Q_l = 0.099 LPM (Re_l = 1000), Q_g = 0 LPM (Re_g = 0 LPM), which produces a laminar stream of liquid. This condition is shown in Figure 4 as imaged with the white beam at APS and in Figure 5 as imaged with the monochromatic beam at APS, both immediately downstream of the nozzle exit. Both images have been normalized to remove as much background intensity variation as is possible with current algorithms. It can be seen clearly that the white beam image contains a much lower level of background noise than the mono beam image. However, because the mono beam is more strongly absorbed by water than the white beam, there is more contrast between the background and the liquid stream in the mono beam. It should also be noted that the higher power of the white beam permits the use of a much shorter exposure time (1.05 μs) than the mono beam image (278 μs). At this condition, the flow is stable and the few perturbations that do occur result in slow transients. Therefore, the comparatively long exposure of the mono beam image is not an issue.

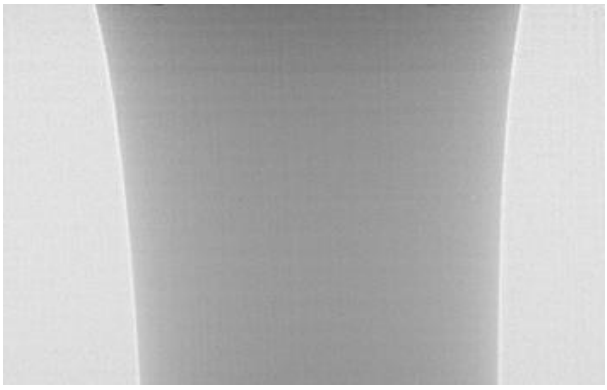

Figure 4 White beam image of a laminar liquid stream with Re_l = 1000. The top of the image corresponds to the nozzle exit and spans a width of 3.4 mm and height of 2.1 mm.

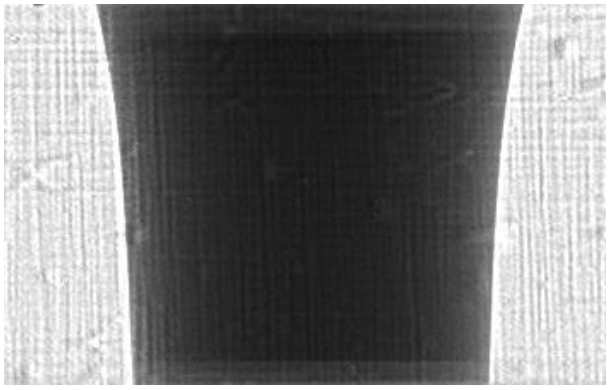

Figure 5 Mono beam image of a laminar liquid stream with Re_l = 1000. The top of the image corresponds to the nozzle exit and spans a width of 3.4 mm and height of 2.1 mm.

The second flow condition tested was Q_l = 0.099 LPM (Re_l = 1000), Q_g =150 LPM (Re_g = 16,709), which results in a low velocity spray. Figure 6 shows a white beam image of this condition (1.05 μs exposure) and Figure 7 shows a mono beam image (139 μs exposure) of this condition, both at approximately 5 mm downstream of the nozzle exit. Again, both images have been normalized to remove as much background intensity variation as possible. In addition to the previously noted disparity in background noise, the higher velocity transients in this condition also cause motion blur in the mono beam image, which is not present in the white beam image due to the extremely short exposure time. This motion blur introduces the potential for the EPL to be underestimated due to dynamic bias error [2,11].

Unlike the white beam image, the EPL can be calculated directly from the mono beam image. While this information can be used in multiple ways, e.g. to measure the shape of droplets, one method of analysis is to calculate the time-averaged effective path length, or mean EPL. Using Equation (5), the mean EPL can be calculated from the mono beam data and compared to the same information as acquired by a focused beam raster scan. Figure 8 shows the mean EPL from both mono beam radiography and focused beam radiography at a position of y = 0.5 mm downstream of the nozzle exit for the laminar water stream condition. Similarly, Figure 9 shows the mean EPL from both mono beam radiography and a focused beam radiography scan for the low velocity spray at a position of y = 1.0 mm downstream of the nozzle exit. In both conditions, the mean EPL profiles match well between the mono beam and focused beam information. The largest discrepancy in mean EPL between the mono beam radiography and the focused beam radiography occurs at the edges of the low velocity spray (around $x = -1.0$ mm and $x = 1.0$ mm). The most likely cause of this discrepancy is that the long exposure time of the

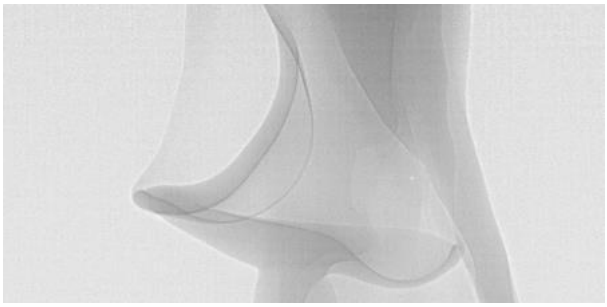

Figure 6 A white beam image of low velocity spray with Re_l = 1000 and Re_g = 16,700. The top of the image is approximately 5 mm below the nozzle exit and spans a width of 4.2 mm and a height of 2.1 mm.

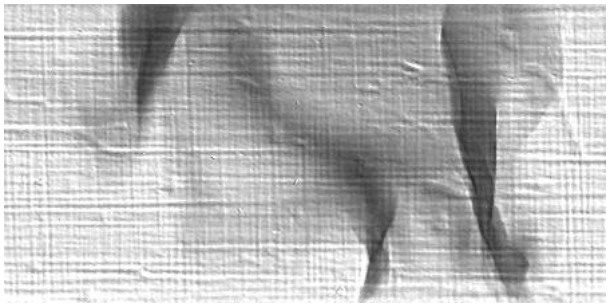

Figure 7 A mono beam image of a low velocity spray with Re_l = 1000 and Re_g = 16,700. The top of the image is approximately 5 mm below the nozzle exit and spans a width of 4.2 mm and a height of 2.1 mm.

mono beam radiography is too slow to capture the high-speed dynamics in this high-shear zone, resulting in a small dynamic bias error. Additionally, the focused beam information is much lower in noise than the mono beam image. This lower noise comes at the expense of a long raster scanning process. Each of the 49 averaged data points in the focused beam scan in Figure 8 required 10 s to acquire, whereas the 736 averaged data points in the mono beam in Figure 8 (along with the data points for over 200 more axial locations) were acquired in a single 3 s imaging sequence.

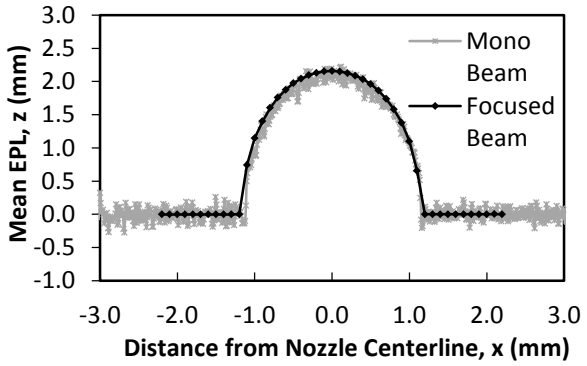

Figure 8 The mean EPL through the laminar water stream (Re_l = 1000, Re_g = 0) at 0.5 mm downstream from the nozzle exit.

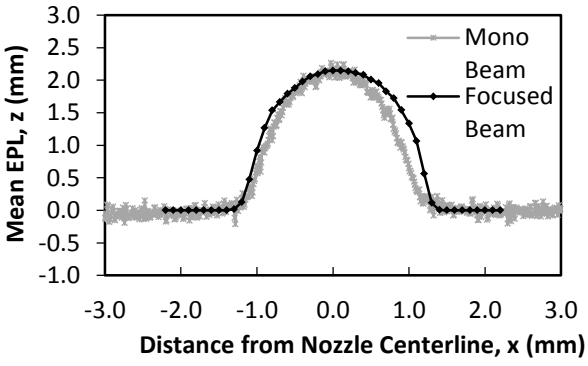

Figure 9 The mean EPL through the low velocity spray (Re_l = 1000, Re_g = 16,700) at 1 mm downstream from the nozzle exit.

Conclusions

Monochromatic X-ray imaging of sprays has great potential to provide detailed information about the dense liquid region near the nozzle exit of sprays where visible light cannot penetrate. Mono beam radiography provides the EPL determining capability of focused beam radiography, while maintaining the capability to measure the spatial-temporal structures that white beam radiography captures. However, it has also been shown that significant challenges remain to be overcome. Specifically, the moving background introduced by the combination of the X-ray source movement and the vibrations in the monochromator causes non-trivial noise to the images, which both lowers the visual quality of the images as compared to white beam radiography as well as reduces the precision of the data as compared to focused beam radiography. Additionally, the low intensity of the X-ray beam as compared to white beam radiography necessitates the use of much longer image exposure times, which introduces motion blur into the images and creates the potential for dynamic bias error. Further work will be necessary to determine if algorithms can be developed to satisfactorily remove the moving background; however, reductions in motion blur will likely require the development of more powerful monochromatic X-ray sources.

Acknowledgments

This work was sponsored by the Office of Naval Research (ONR) as part of the Multidisciplinary University Research Initiatives (MURI) Program, under grant number N00014-16-1-2617. The views and conclusions

contained herein are those of the authors only and should not be interpreted as representing those of ONR, the U.S. Navy, or the U.S. Government.

This work was performed at the 7-BM beamline of the Advanced Photon Source, a U.S. Department of Energy (DOE) Office of Science User Facility operated for the DOE Office of Science by Argonne National Laboratory under Contract No. DE-AC02-06CH11357.

References

[1] Heindel T. J., 2011, "A Review of X-ray Flow Visualization with Applications to Multiphase Flows," ASME J. Fluids Eng., **133**(7), p. 74001.

[2] Kastengren A., and Powell C. F., 2014, "Synchrotron X-ray Techniques for Fluid Dynamics," Exp. Fluids, **55**(3), p. 1686.

[3] MacPhee A. G., Tate M. W., Powell C. F., Yue Y., Renzi M. J., Ercan A., Narayanan S., Fontes E., Walther J., Schaller J., Gruner S. M., and Wang J., 2002, "X-ray Imaging of Shock Waves Generated by High-Pressure Fuel Sprays," Science (80-.)., **295**(5558), pp. 1261–1263.

[4] Wang J., 2005, "X-ray Vision of Fuel Sprays," J. Synchrotron Radiat., **12**(2), pp. 197–207.

[5] Halls B. R., Heindel T. J., Kastengren A. L., and Meyer T. R., 2014, "Evaluation of X-ray Sources for Quantitative Two- and Three-Dimensional Imaging of Liquid Mass Distribution in Atomizing Sprays," Int. J. Multiph. Flow, **59**, pp. 113–120.

[6] Machicoane N., and Aliseda A., 2017, "Experimental Characterization of a Canonical Coaxial Gas-Liquid Atomizer," ILASS-Americas 29th Annual Conference on Liquid Atomization and Spray Systems, Atlanta, GA, USA.

[7] Bothell J. K., Li D., Morgan T. B., Heindel T. J., Aliseda A., Machicoane N., and Kastengren A. L., 2018, "Characterizing the Near-Field Region of a Spray using White Beam and Focused Beam X-ray Measurements," ICLASS 2018, 14th Triennial International Conference on Liquid Atomization and Spray Systems, Chicago, IL, USA.

[8] Li D., Bothell J. K., Morgan T. B., Heindel T. J., Aliseda A., Machicoane N., and Kastengren A. L., 2018, "Quantitative Analysis of an Airblast Atomizer Near-Field Region using Broadband and Narrowband X-ray Sources," ICLASS 2018, 14th Triennial International Conference on Liquid Atomization and Spray Systems, Chicago, IL, USA.

[9] Berger M. J., Hubbell J. H., Seltzer S. M., Chang J., Coursey J. S., Sukumar R., Zucker D. S., and Olsen K., 2010, "XCOM: Photon Cross Section Database," Natl. Inst. Stand. Technol. [Online]. Available: http://physics.nist.gov/xcom. [Accessed: 26-Feb-2018].

[10] Emery L., and Borland M., 1999, "Top-Up Operation Experience at the Advanced Photon Source," Proceedings of the 1999 Particle Accelerator Conference (Cat. No.99CH36366), IEEE, New York, NY, USA, pp. 200–202 vol.1.

[11] Andersson P., Sundén E. A., Jacobsson Svärd S., and Sjöstrand H., 2012, "Correction for Dynamic Bias Error in Transmission Measurements of Void Fraction," Rev. Sci. Instrum., **83**(12), p. 125110.